2017-10

Combined web distortional and lateral-torsional buckling of partially restrained I-section beams

Lei, J-S

10.1016/j.ijmecsci.2017.06.057
International Journal of Mechanical Sciences
Elsevier BV

International Journal of Mechanical Sciences 131–132 (2017) 107–112
http://dx.doi.org/10.1016/j.ijmecsci.2017.06.057
Accepted 30 June 2017

Combined web distortional and lateral-torsional buckling of partially restrained I-section beams

Jin-song Lei[a,b], Long-yuan Li[c]

a) College of Civil Engineering and Architecture, Southwest University of Science and Technology, Mianyang 621010, China (leijinsong@swust.edu.cn)
b) Shock and Vibration of Engineering Materials and Structures Key Laboratory of Sichuan Province, Southwest University of Science and Technology, Mianyang 621010, China
c) School of Engineering, University of Plymouth, Plymouth PL4 8AA, UK (long-yuan.li@plymouth.ac.uk)

Abstract - This paper proposes an analytical model for analyzing the interaction between web distortion and lateral-torsional buckling of partially restrained I-section beams under transverse distribution loading. The analysis is performed by using Rayleigh-Ritz method, in which the web is modelled as a plate and the two flanges are treated as two independent beams. The total potential energy functional of the system is derived using three-dimensional strain-displacement relationships in solid mechanics. The critical buckling stress and critical buckling moment of the I-section beam are calculated by solving a 3x3 eigen-matrix equation. For the validation of the present model the finite element analysis using three-dimensional shell elements is also carried out. The comparison between the analytical and numerical results demonstrates the correctness and rigorous of the proposed analytical model despite its simplicity.

Keywords: I-section, beam, web distortional buckling, lateral-torsional buckling.

1. Introduction

It is well-known that beams, which have a large flexural rigidity in their loaded plane and a small flexural rigidity in the other plane, such as I-section beams and castellated beams, are prone to web distortional buckling [1-9] and/or lateral-torsional buckling [10-26] depending on lateral restraint conditions and the slenderness of the flanges and web of the beams. The load, at which the buckling occurs, may be considerably less than the in-plane load-carrying capacity of the beam. Note that the web distortional buckling generally occurs in beams in which the tension flange is fully or partially restrained in the lateral direction of the beams and the compression flange is completely free; whereas the lateral-torsional buckling frequently occurs in beams which have no lateral and/or rotational restraints. The former is characterized by the rotation and translation of the free flange, which is in compression, with a distortion in the web; whereas the latter is

characterized by the lateral deflection and sectional rotation of the beam along its length direction without cross-sectional distortion. In some cases the beam may buckle in a combined mode of web distortion and lateral-torsional buckling, in which case the interaction exists between the two buckling modes [27-30].

The elastic lateral-torsional buckling problem of I-beams was first studied by Timoshenko and Gere [1] using analytical method. Following Timoshenko and Gere work, many researchers have investigated the lateral-torsional buckling of beams of different types. For instance, Ings and Trahair [2] investigated the lateral buckling of restrained roof purlins. Collin et al. [3] discussed the lateral-torsional buckling of continuous bridge girders. Özdemir and Topkaya [4] examined the lateral buckling of overhanging crane trolley monorails. Andrade et al. [5] studied the lateral-torsional buckling of singly symmetric web-tapered thin-walled I-beams. Kurniawan and Mahendran [6], Anapayan and Mahendran [7] investigated the elastic lateral buckling of LiteSteel beams subjected to transverse loading. Sweedan [8] and Panedpojaman et al. [9] investigated the elastic lateral stability and the inelastic lateral–torsional buckling of cellular steel beams, respectively.

Unlike the sole lateral-torsional buckling, most of work on buckling of beams involving web distortion started only in 1990s. For example, Wang et al. [10] provided a parametric study on the distortional buckling of monosymmetric structural members. Ma and Hughes [11], Samanta and Kumar [12] investigated the lateral distortional buckling of monosymmetric I-beams subjected to transverse load. Kolakowski et al. [13] discussed the modal interactive buckling of thin-walled composite beam-columns concerning distortional deformations. Teter and Kolakowski [14] investigated the interactive buckling and load carrying capacity of beam–columns with intermediate stiffeners. Vrcelj and Bradford [15] examined the elastic distortional buckling of doubly symmetric steel I-section members with thin webs and stocky flanges, in which their tension flange is fully restrained against the translational and lateral rotational buckling deformations and elastically restrained against the twist rotation. White and Jung [16] discussed the effect of web distortion on the buckling strength of noncomposite discretely-braced steel I-section members. Zirakian [17] provided a comparison of elastic distortional buckling strengths of doubly symmetric I-shaped flexural members with slender webs by using AISC code prediction and finite strip analysis. Trahair [18,19] investigated the lateral-distortional buckling of normal and overhanging monorail I-beams and its influence on the design strengths of the beams. Anapayan et al. [20], Anapayan and Mahendran [21] investigated the lateral distortional buckling of LiteSteel beams using experimental and numerical methods. Kalkan and Buyukkaragoz [22] presented an analytical and numerical study on the distortional buckling of doubly-symmetric steel I-beams. Gonçalves [23] provided a geometrically exact approach to analyzing the lateral-torsional buckling of thin-walled beams with deformable cross-section. Hassanein and Silvestre [24] discussed the lateral–distortional buckling of hollow tubular flange plate girders with slender unstiffened webs. Yuan et al. [25] and Tong et al. [26] investigated the flange-web distortional buckling of thin-walled beams under different restraint conditions.

Interaction between the lateral-torsional buckling and the web distortional buckling of channel- and hat-sections was investigated by Schardt [27] using the generalized beam theory. Bradford [28] studied the interactive buckling of beams with continuous and completely restrained tension flange by using a special-purpose inelastic finite element analysis method. Ellobody [29,30] investigated the behaviour of normal and high strength castellated and cellular steel beams under combined lateral-torsional and distortional buckling modes using a nonlinear finite element analysis method. His results showed that the cellular steel beams failing due to combined web distortional and web-post buckling modes exhibited a significant decrease in failure loads. Recently, Kim et al. [31] proposed an analytical model for calculating the lateral-torsional critical transverse load of castellated beams. More recently, Zhu and Li [32] and Huang and Zhu [33] investigated the distortional buckling problems of thin-walled steel beams and columns using the stiffened plate buckling model, which considers the interaction between the web and flange. Yuan et al. [34] studied the distortional buckling of perforated cold-formed steel channel-section beams with circular holes in web, which also considers the interaction between the web and flange.

In practice, there are many I-section beams that are partially restrained, largely in lateral and rotational directions. In a beam-roof system, for instance, the beam is usually restrained by the roof in its lateral direction. Under the action of uplift wind load, the bottom flange of the beam is in compression, whereas the top flange of the beam, which is restrained by the roof, is in tension. The buckling behavior of such partially restrained beams is different from that of unrestrained beams. The second example is the I-section beam used to support the composite floor. During concrete casting the beam is bent under the gravity load; while its bottom flange is in tension and is restrained by the steel deck and its top flange is in compression and is entirely free. If the flexural rigidity of the beam about its minor axis is small or the web of the I-beam is weak, then the web distortional buckling and/or the lateral-torsional buckling of the beam may occur during the construction of the composite floor. This kind of buckling problems is not fully addressed and there is no direct equation or formula that can be utilized to determine the critical load to characterize the web distortional buckling and/or the lateral-torsional buckling of partially restrained I-section beams subjected to transverse distribution loading. In this paper an analytical approach is proposed to analyze the web distortional and lateral-torsional buckling problem of partially restrained I-section beams subjected to transverse distribution loading. The buckling analysis is performed by using the Rayleigh-Ritz method, in which the web is modelled as a plate and the two flanges are treated as two independent beams. The total potential energy of the system is derived using the three-dimensional strain-displacement relationships in solid mechanics. To validate the present analytical model, finite element analyses using three-dimensional shell elements are also carried out. The comparison between the analytical and numerical results demonstrates the correctness and rigorous of the proposed analytical model despite its simplicity.

2. Combined web-distortional and lateral-torsional buckling model

Consider an I-section beam subjected to a uniformly distributed gravity load. Assume that the bottom flange of the beam is completely restrained in its lateral direction and partially restrained in its rotational direction. Let b_f and t_f be the width and thickness of the flanges, h_w and t_w be the depth and thickness of the web (see Figure 1a). Under the action of the gravity loading, the upper flange of the beam, which is free, is in compression and the bottom flange of the beam, which is partially restrained, is in tension. Hence, when the load reaches to a certain level, the beam will have a lateral-torsional buckling involving web distortion because of the effect of restraints applied at the bottom flange (see Figure 1b). This kind of buckling mode is different from the traditional lateral-torsional buckling mode which does not involve web distortion.

Assume that the lateral-torsional buckling mode of the beam with web distortion can be characterized by the translational displacement, w_1, and the rotational displacements, ϕ_1 and ϕ_2 of the upper and bottom flanges (see Figure 1b). To determine the critical load that is associated with the assumed buckling modes, the total potential energy change of the system owing to the assumed buckling displacements is evaluated. For the simplicity of presentation, the I-section is divided into three components, namely the free flange, the restrained flange, and the web. During the lateral-torsional buckling with web distortion the web is assumed to behave like a plate and the free and restrained flanges are assumed to behave like independent beams. According to the displacements defined in Figure 1b, the free flange has a translational displacement w_1 and a rotational displacement ϕ_1. Hence the strain energy of the free flange can be expressed as follows,

$$U_1 = \frac{Et_f b_f^3}{24}\int_o^l \left(\frac{d^2 w_1}{dx^2}\right)^2 dx + \frac{Gb_f t_f^3}{6}\int_o^l \left(\frac{d\phi_1}{dx}\right)^2 dx \qquad (1)$$

where E is the Young's modulus, G is the shear modulus, and l is the beam length. In contrast, the restrained flange has only a rotational displacement ϕ_2, and its strain energy can be expressed as follows,

$$U_2 = \frac{Gb_f t_f^3}{6}\int_o^l \left(\frac{d\phi_2}{dx}\right)^2 dx + \frac{k_\phi}{2}\int_o^l \phi_2^2 \qquad (2)$$

where k_ϕ in N-m/m is the rotational spring constant per unit length. The second term in Eq. (2) is the strain energy of the rotational spring provided by the restraint, such as from the roof or floor supported by the beam. The strain energy of the web can be calculated using the bending theory of plates as follows,

$$U_3 = \frac{D}{2}\int_o^l\int_o^{h_w}\left[\left(\frac{\partial^2 w_3}{\partial x^2}+\frac{\partial^2 w_3}{\partial y^2}\right)^2 + 2(1-\nu)\left(\left(\frac{\partial^2 w_3}{\partial x \partial y}\right)^2 - \frac{\partial^2 w_3}{\partial x^2}\frac{\partial^2 w_3}{\partial y^2}\right)\right]dxdy \qquad (3)$$

where $D = \dfrac{Et_w^3}{12(1-\nu^2)}$ is the flexural rigidity of the web plate, ν is the Poisson's ratio, and w_3 is the deflection function of the web plate, defined as

$$w_3(x,y) = N_1(y)w_1 - N_2(y)\phi_1 - N_3(y)\phi_2 \qquad (4)$$

where $N_j(y)$ (j = 1, 2, 3) are the interpolation functions, which are defined by Eqs.(5)-(7),

$$N_1(y) = 1 - 3\left(\frac{y}{h_w}\right)^2 + 2\left(\frac{y}{h_w}\right)^3 \tag{5}$$

$$N_2(y) = h_w\left[\frac{y}{h_w} - 2\left(\frac{y}{h_w}\right)^2 + \left(\frac{y}{h_w}\right)^3\right] \tag{6}$$

$$N_3(y) = -h_w\left[\left(\frac{y}{h_w}\right)^2 - \left(\frac{y}{h_w}\right)^3\right] \tag{7}$$

For the uniformly distributed load, the pre-buckling stresses involve both the bending and shear stresses. They can be calculated using the theory of beams as follows,
In the free flange:

$$\sigma_{1x} = \frac{q_{cr} l(h_w + t_f)x}{4I_z}\left(1 - \frac{x}{l}\right) = 4\sigma_{cr}\left(\frac{x}{l}\right)\left(1 - \frac{x}{l}\right) \tag{8}$$

$$\tau_{1xz} = \frac{q_{cr} l(h_w + t_f)}{4I_z}\left(\frac{b_f}{2} - |z|\right)\left(1 - \frac{2x}{l}\right) sign(z) = \frac{4\sigma_{cr}}{l}\left(\frac{b_f}{2} - |z|\right)\left(1 - \frac{2x}{l}\right) sign(z) \tag{9}$$

where σ_{1x} and τ_{1xz} are the compressive and shear stresses in the free flange, q_{cr} is the critical density of the uniformly distributed load, I_z is the second moment of the area of the I-beam about its major axis, sign(z) = 1 for $z > 0$ and sign(z) = -1 for $z < 0$ is the sign function, and σ_{cr} is the largest bending stress occurs at $x = l/2$ and $y = 0$ when buckling occurs and defined as,

$$\sigma_{cr} = \frac{q_{cr} l^2 (h_w + t_f)}{16 I_z} \tag{10}$$

In the restrained flange:

$$\sigma_{2x} = -\sigma_{1x} \tag{11}$$

$$\tau_{2xz} = -\tau_{1xz} \tag{12}$$

where σ_{2x} and τ_{2xz} are the compressive and shear stresses in the restrained flange.

In the web:

$$\sigma_{3x} = \sigma_{1x}\left(1 - \frac{2y}{h_w}\right) \tag{13}$$

$$\tau_{3xy} \approx -\frac{q_{cr} l}{2h_w t_w}\left(1 - \frac{2x}{l}\right) = -\frac{8\sigma_{cr} I_z}{h_w t_w (h_w + t_f) l}\left(1 - \frac{2x}{l}\right) \tag{14}$$

The loss of potential of the prebuckling stresses in the two flanges and web is respectively expressed as follows,

$$W_1 = \frac{b_f t_f}{2}\int_o^l \sigma_{1x}\left[\left(\frac{dw_1}{dx}\right)^2 + \left(r_{c1}\frac{d\phi_1}{dx}\right)^2\right]dx + \frac{t_f}{2}\int_0^l \int_{-b_f/2}^{b_f/2} 2\tau_{1xz}\frac{d(z\phi_1)}{dx}\frac{d(z\phi_1)}{dz}dzdx \tag{15}$$

$$W_2 = \frac{b_f t_f}{2}\int_o^l \sigma_{2x}\left(r_{c2}\frac{d\phi_2}{dx}\right)^2 dx + \frac{t_f}{2}\int_0^l\int_{-b_f/2}^{b_f/2} 2\tau_{2xz}\frac{d(z\phi_2)}{dx}\frac{d(z\phi_2)}{dz}dzdx \tag{16}$$

$$W_3 = \frac{t_w}{2}\int_o^l\int_o^{h_w} \sigma_{3x}\left(\frac{\partial w_3}{\partial x}\right)^2 dxdy + \frac{t_w}{2}\int_o^l\int_o^{h_w} 2\tau_{3xy}\left(\frac{\partial w_3}{\partial x}\right)\left(\frac{\partial w_3}{\partial y}\right)dxdy \tag{17}$$

where $r_{c1} = r_{c2} = \frac{1}{2}\sqrt{\frac{t_f^2 + b_f^2}{3}}$ is the polar radius of gyration of the free/restrained flange.

Note that if the applied load is not applied at the shear centre of the I-section beam then the loss of the potential of the applied load needs to be considered, which can be expressed as follows,

$$W_4 = \frac{q_{cr}}{2}\int_o^l\int_o^{h_w/2}\left(\frac{\partial w_3}{\partial y}\right)^2 dxdy \qquad \text{for load applied at upper flange} \tag{18}$$

or

$$W_4 = -\frac{q_{cr}}{2}\int_o^l\int_{h_w/2}^{h_w}\left(\frac{\partial w_3}{\partial y}\right)^2 dxdy \qquad \text{for load applied at lower flange} \tag{19}$$

The translational displacement, w_1, and the rotational displacements, ϕ_1 and ϕ_2 of the upper and bottom flanges of the beam are assumed as follows,

$$w_1(x) = C_1 \sin\frac{k\pi x}{l} \tag{20}$$

$$\phi_1(x) = C_2 \sin\frac{k\pi x}{l} \tag{21}$$

$$\phi_2(x) = C_3 \sin\frac{k\pi x}{l} \tag{22}$$

where C_j (j = 1, 2, 3) are the constants, and k is the number of half-waves. It is known that when the buckling occurs the total potential of the system will have a stationary condition with respect to the constants C_1, C_2 and C_3, that is,

$$\frac{\partial \Pi}{\partial C_1} = \frac{\partial}{\partial C_1}\left(U_1 + U_2 + U_3 - W_1 - W_2 - W_3 - W_4\right) = 0 \tag{23}$$

$$\frac{\partial \Pi}{\partial C_2} = \frac{\partial}{\partial C_2}\left(U_1 + U_2 + U_3 - W_1 - W_2 - W_3 - W_4\right) = 0 \tag{24}$$

$$\frac{\partial \Pi}{\partial C_3} = \frac{\partial}{\partial C_3}\left(U_1 + U_2 + U_3 - W_1 - W_2 - W_3 - W_4\right) = 0 \tag{25}$$

Substituting Eqs. (20)-(22) into (1)-(3) and (15)-(19), then into (23)-(25), it yields

$$\begin{bmatrix} A_{11} & A_{12} & A_{13} \\ A_{21} & A_{22} & A_{23} \\ A_{31} & A_{32} & A_{33} \end{bmatrix}\begin{Bmatrix} C_1 \\ C_2 \\ C_3 \end{Bmatrix} = \sigma_{cr}\begin{bmatrix} B_{11} & B_{12} & B_{13} \\ B_{21} & B_{22} & B_{23} \\ B_{31} & B_{32} & B_{33} \end{bmatrix}\begin{Bmatrix} C_1 \\ C_2 \\ C_3 \end{Bmatrix} \tag{26}$$

in which

$$A_{11}=\frac{2}{l}\left(\frac{l}{k\pi}\right)^2\frac{\partial^2 U}{\partial C_1^2}=\frac{Eb_f^3t_f}{12}\left(\frac{k\pi}{l}\right)^2+\frac{13h_wD}{35}\left(\frac{k\pi}{l}\right)^2+\frac{12D}{5h_w}+\frac{12D}{h_w^3}\left(\frac{l}{k\pi}\right)^2 \quad (27)$$

$$A_{12}=A_{21}=\frac{2}{l}\left(\frac{l}{k\pi}\right)^2\frac{\partial^2 U}{\partial C_1\partial C_2}=-\frac{11h_w^2D}{210}\left(\frac{k\pi}{l}\right)^2-\frac{6D}{5}-\frac{6D}{h_w^2}\left(\frac{l}{k\pi}\right)^2+D(1-\nu) \quad (28)$$

$$A_{13}=A_{31}=\frac{2}{l}\left(\frac{l}{k\pi}\right)^2\frac{\partial^2 U}{\partial C_1\partial C_3}=\frac{13h_w^2D}{420}\left(\frac{k\pi}{l}\right)^2-\frac{D}{5}-\frac{6D}{h_w^2}\left(\frac{l}{k\pi}\right)^2 \quad (29)$$

$$A_{22}=\frac{2}{l}\left(\frac{l}{k\pi}\right)^2\frac{\partial^2 U}{\partial C_2^2}=\frac{Gb_ft_f^3}{3}+\frac{h_w^3D}{105}\left(\frac{k\pi}{l}\right)^2+\frac{4h_wD}{15}+\frac{4D}{h_w}\left(\frac{l}{k\pi}\right)^2 \quad (30)$$

$$A_{23}=A_{32}=\frac{2}{l}\left(\frac{l}{k\pi}\right)^2\frac{\partial^2 U}{\partial C_2\partial C_3}=-\frac{h_w^3D}{140}\left(\frac{k\pi}{l}\right)^2-\frac{h_wD}{15}+\frac{2D}{h_w}\left(\frac{l}{k\pi}\right)^2 \quad (31)$$

$$A_{33}=\frac{2}{l}\left(\frac{l}{k\pi}\right)^2\frac{\partial^2 U}{\partial C_3^2}=\frac{Gb_ft_f^3}{3}+k_\phi\left(\frac{l}{k\pi}\right)^2+\frac{h_w^3D}{105}\left(\frac{k\pi}{l}\right)^2+\frac{4h_wD}{15}+\frac{4D}{h_w}\left(\frac{l}{k\pi}\right)^2 \quad (32)$$

$$B_{11}=\frac{2}{l}\left(\frac{l}{k\pi}\right)^2\frac{\partial^2 W}{\partial C_1^2}=\left(b_ft_f+\frac{h_wt_w}{5}\right)\left(\frac{2}{3}-\frac{2}{(k\pi)^2}\right)+\frac{8(5+6\alpha-6\beta)I_z}{5h_w(h_w+t_f)(k\pi)^2} \quad (33)$$

$$B_{12}=B_{21}=\frac{2}{l}\left(\frac{l}{k\pi}\right)^2\frac{\partial^2 W}{\partial C_1\partial C_2}=-\frac{2h_w^2t_w}{105}\left(\frac{2}{3}-\frac{2}{(k\pi)^2}\right)+\frac{(7\alpha+23\beta)I_z}{10(h_w+t_f)(k\pi)^2} \quad (34)$$

$$B_{13}=B_{31}=\frac{2}{l}\left(\frac{l}{k\pi}\right)^2\frac{\partial^2 W}{\partial C_1\partial C_3}=\frac{h_w^2t_w}{420}\left(\frac{2}{3}-\frac{2}{(k\pi)^2}\right)-\frac{(23\alpha+7\beta)I_z}{10(h_w+t_f)(k\pi)^2} \quad (35)$$

$$B_{22}=\frac{2}{l}\left(\frac{l}{k\pi}\right)^2\frac{\partial^2 W}{\partial C_2^2}=\left(r_{c1}^2b_ft_f+\frac{h_w^3t_w}{420}\right)\left(\frac{2}{3}-\frac{2}{(k\pi)^2}\right)+\frac{b_f^3t_f}{3(k\pi)^2}+\frac{(47\alpha-17\beta)I_z}{30(k\pi)^2} \quad (36)$$

$$B_{23}=B_{32}=\frac{2}{l}\left(\frac{l}{k\pi}\right)^2\frac{\partial^2 W}{\partial C_2\partial C_3}=-\frac{4(\alpha-\beta)I_zh_w}{15(h_w+t_f)(k\pi)^2} \quad (37)$$

$$B_{33}=\frac{2}{l}\left(\frac{l}{k\pi}\right)^2\frac{\partial^2 W}{\partial C_3^2}=-\left(r_{c2}^2b_ft_f+\frac{h_w^3t_w}{420}\right)\left(\frac{2}{3}-\frac{2}{(k\pi)^2}\right)-\frac{b_f^3t_f}{3(k\pi)^2}+\frac{(17\alpha-47\beta)h_wI_z}{30(h_w+t_f)(k\pi)^2} \quad (38)$$

where $U = U_1 + U_2 + U_3$, $W = W_1 + W_2 + W_3 + W_4$, α and β are the factors of either equal to zero or one, depending on the loading position. For the load applied at mid of the web W_4=0 and thus $\alpha = 0$, $\beta = 0$. For the load applied at upper flange W_4 is defined by Eq.(18) and thus $\alpha = 1$, $\beta = 0$. For the load applied at lower flange W_4 is defined by Eq.(19) and thus $\alpha = 0$, $\beta = 1$.

Eq. (26) presents an eigen-value equation from which the critical stress σ_{cr} can be determined. The critical load q_{cr} can be calculated directly using Eq. (10) from the obtained σ_{cr}. Note that the present model considers not only the bending stress but also the shear stress. The latter could be very important in the web distortional buckling of short beams.

3. Numerical examples

As numerical examples, herein three I-section beams of different flange widths are discussed, which represent the narrow, modest and wide flange-beams. In all cases the uniform transverse load is assumed to act at the shear centre. Figures 2-4 show the calculated critical buckling stresses of the three beams from the present model. In each case three different rotational spring constants are considered.

It can be seen from Figure 2 that, the critical stress of the narrow beam without rotational restraint drops continuously with the increase of beam length. In contrast, the critical stress of the beams with rotational restraint drops initially and then increases with the increase of beam length. The latter reflects the influence of the rotational restraint on the lateral-torsional buckling and web distortional buckling of the beam. Note that if there is no rotational restraint the beam can rotate freely and when the buckling occurs the rotational and translational displacements will adjust themselves automatically from all admissible displacements to achieve the buckling mode associated to the smallest buckling load. However, when the rotational restraint is applied, the adjustment of the rotational and translational displacements for developing possible buckling mode is limited largely by the rotational displacement, which leads to a significant change in the configuration of buckling curve. It can also be found from the figure that, the lowest critical stress increases with increased rotational spring constant; whereas the characteristic length of the beam corresponding to the lowest critical stress reduces with increased rotational spring constant. This feature is similar to the local and distortional buckling happened in most cold-formed steel members, for which the minimum critical stresses are related to the wavelengths of their buckling modes which define the critical loads of local buckling and distortional buckling. Therefore, for a partially restrained I-section beam, one can use the minimum critical stress for the design for the lateral-torsional and web distortional buckling of the beam if the rotational restraint at its tension flange is sufficiently large.

Figures 3 and 4 show the critical buckling stresses of the modest and wide flange beams with different rotational spring constants. The main buckling behavior of these two beams is similar to that of the narrow flange beam shown in Figure 2. Comparing the critical stresses shown in Figures 2 and 3 or in Figures 3 and 4, one can see the critical stress increases with the flange width, which is to be expected. For example, the critical stress ratios of the narrow, modest and wide flange beams of 8 m beam length are 0.423, 0.553, and 0.740 for k_ϕ = 0; 0.470, 0.592, and 0.773 for k_ϕ = 500 N; and 0.564, 0.667, and 0.835 for k_ϕ = 1500 N, respectively. However, the influence of the rotational spring constant k_ϕ on the critical stress decreases with the increase of flange width. For example, the increase of critical stress for k_ϕ from 0 to 500 N is 11%, 6.9% and 4.3% in the the narrow, modest and wide flange beams. While, the increase of critical stress for k_ϕ from 0 to 1500 N is 33%, 20% and 13% in the the narrow, modest and wide flange beams. This indicates that for beams of wider flanges one should use stronger rotational restraints in

order to increase the buckling resistance of the beams against the web distortional buckling and/or lateral-torsional buckling.

In order to validate the aforementioned analytical model, finite element analyses are also conducted by using ANSYS software. The three I-section beams of various lengths used in the above-mentioned examples are analyzed numerically using three-dimensional shell elements (shell 181) built in ANSYS software. The material properties used in the finite element analyses are Young's modulus of E=210GPa and Poisson's ratio of ν=0.3. Owing to geometric symmetry, only a half span of the beam is modelled. The boundary conditions of the beam are assumed as that: the nodes on one end section of the beam (x = 0) have zero transverse and lateral displacements ($v = w = 0$) and on the other end section of the beam (symmetric section at $x = l/2$) have zero rotations about the transverse and lateral axes ($\phi_y = \phi_z = 0$) and zero axial displacement ($u = 0$). In addition, zero lateral displacement ($v = 0$) is applied to the nodes on the intersection line between the tension flange and web to simulate the lateral displacement restraint. The transverse load is applied at the top of the web connected to the compression flange.

Linear buckling analysis is utilized to find the smallest positive eigenvalue, which represents the critical load of the beam when the transverse load is applied at the top flange. The largest element size of mesh used in the finite element analysis is 20 mm. This is determined from several trials, which show the eigen-values associated to the first two lowest buckling modes having virtually no change with the reduction in mesh sizes.

Figure 5 shows a comparison of critical moments, $M_{cr} = q_{cr}l^2/8$, of the narrow, modest and wide flange beams obtained from the present analytical model and finite element analyses. It is evident from the figure that the results obtained from the present analytical model be in excellent agreement with those computed from the finite element analysis. This demonstrates that the use of the plate model for the web and the independent beam model for the two flanges proposed in the present study is appropriate and able to characterize the interaction of web distortional buckling and lateral-torsional buckling of the partially restrained I-section beam.

4. Conclusions

This paper has presented an analytical model for analysing the web distortional buckling and lateral-torsional buckling of partially restrained I-section beams subjected to transverse distribution loading. The analysis is performed by using Rayleigh-Ritz approach, in which the web is treated as a plate and the two flanges are modelled as independent beams. The potential energy functional of the system is derived using the three-dimensional strain-displacement relationships in solid mechanics. The finite element analysis has also been used to validate the critical load or critical moment calculated from the present model. From the obtained results the following conclusions can be drawn:

- The lateral and rotational restraints applied at the tension-flange of an I-section beam can considerably increase the critical load of the beam, particularly to the long span beam.
- Not only can the rotational restraint increase the critical load of web distortional and lateral-torsional buckling but also can shaft the critical buckling mode from lateral-torsional buckling to web distortional buckling.
- When the web distortional buckling becomes a significant part in the critical buckling mode the buckling stress curve of the partially restrained beam will exhibit a minimal point. Before the minimal point the critical stress decreases, but after the minimal point it increases with the beam length.
- The level of increase in critical buckling stress/moment due to the use of rotational spring is also dependent on the beam size. For the same rotational spring, the beam with narrow flanges has a larger increase in critical load than the beam with wide flanges.

References

[1] S.P. Timoshenko, J. M. Gere, Theory of Elastic Stability (2nd edition), (McGraw-Hill Book Company, New York, 1961).

[2] N.L. Ings, N.S. Trahair, Lateral buckling of restrained roof purlins, Thin-Walled Structures 1984; **2**(4): 285-306.

[3] P. Collin, M. Möller, B. Johansson, Lateral-torsional buckling of continuous bridge girders, Journal of Constructional Steel Research 1998; **45**(2): 217-235.

[4] K.M. Özdemir, C. Topkaya, Lateral buckling of overhanging crane trolley monorails, Engineering Structures 2006; **28**(8): 1162-1172.

[5] A. Andrade, D. Camotim, P.B. Dinis, Lateral-torsional buckling of singly symmetric web-tapered thin-walled I-beams: 1D model vs. shell FEA, Computers & Structures 2007; **85**(17–18): 1343-1359.

[6] C.W. Kurniawan, M. Mahendran, Elastic lateral buckling of simply supported LiteSteel beams subject to transverse loading, Thin-Walled Structures 2009; **47**(1): 109-119.

[7] T. Anapayan, M. Mahendran, Numerical modelling and design of LiteSteel Beams subject to lateral buckling, Journal of Constructional Steel Research 2012; **70**: 51-64.

[8] A.M.I. Sweedan, Elastic lateral stability of I-shaped cellular steel beams, Journal of Constructional Steel Research 2011; **67**(2): 151-163.

[9] P. Pattamad, S.L. Worathep, C.U. Tanan, Cellular beam design for resistance to inelastic lateral–torsional buckling, Thin-Walled Structures 2016; **99**: 182-194.

[10] C.M. Wang, C.K. Chin, S. Kitipornchai, Parametric study on distortional buckling of monosymmetric beam-columns, Journal of Constructional Steel Research 1991; **18**(2): 89-177.

[11] M. Ma and O.F. Hughes, Lateral distortional buckling of monosymmetric I-beams under distributed vertical load. Thin-Walled Structures 1996; **26**(2): 123-145.

[12] A. Samanta, A. Kumar, Distortional buckling in monosymmetric I-beams, Thin-Walled Structures 2006; **44**(1): 51-56.

[13] Z. Kolakowski, M. Krolak, K. Kowal-Michalska, Modal interactive buckling of thin-walled composite beam-columns regarding distortional deformations, International Journal of Engineering Science 1999; **37**(12): 1577-1596.
[14] A. Teter, Z. Kolakowski, Interactive buckling and load carrying capacity of thin-walled beam–columns with intermediate stiffeners, Thin-Walled Structures 2004; **42**(2): 211-254.
[15] Z. Vrcelj, M.A. Bradford, Elastic distortional buckling of continuously restrained I-section beam–columns, Journal of Constructional Steel Research 2006; **62**(3): 223-230.
[16] D.W. White, S.K. Jung, Effect of web distortion on the buckling strength of noncomposite discretely-braced steel I-section members, Engineering Structures 2007; **29**(8): 1872-1888.
[17] T. Zirakian, Elastic distortional buckling of doubly symmetric I-shaped flexural members with slender webs, Thin-Walled Structures 2008; **46**(5): 466-475.
[18] N.S. Trahair, Lateral–distortional buckling of monorails, Engineering Structures 2009; **31**(12): 2873-2879.
[19] N.S. Trahair, Distortional buckling of overhanging monorails, Engineering Structures 2009; **32**(4): 982-987.
[20] T. Anapayan, M. Mahendran, D. Mahaarachchi, Lateral distortional buckling tests of a new hollow flange channel beam, Thin-Walled Structures 2011; **49**(1): 13-25.
[21] T. Anapayan, M. Mahendran, Improved design rules for hollow flange sections subject to lateral distortional buckling, Thin-Walled Structures 2012; **50**(1): 128-140.
[22] I. Kalkan, A. Buyukkaragoz, A numerical and analytical study on distortional buckling of doubly-symmetric steel I-beams, Journal of Constructional Steel Research 2012; **70**: 289-297.
[23] R. Gonçalves, A geometrically exact approach to lateral-torsional buckling of thin-walled beams with deformable cross-section, Computers & Structures 2012; **106–107**: 9-19.
[24] M.F. Hassanein, N. Silvestre, Lateral–distortional buckling of hollow tubular flange plate girders with slender unstiffened webs, Engineering Structures 2013; **56**: 572-584.
[25] W.B. Yuan, S.S. Cheng, L.Y. Li, B. Kim, Web-flange distortional buckling of partially restrained cold-formed steel purlins under uplift loading, International Journal of Mechanical Sciences 2014; **89**: 476-481.
[26] G. Tong, Y. Feng, L. Zhang, A unified analysis for distortional and lateral buckling of C-purlins in flexure, Thin-Walled Structures 2015; **95**: 244-254.
[27] R. Schardt, Lateral torsional and distortional buckling of channel- and hat-sections, Journal of Constructional Steel Research 1994; **31**(2–3): 243-265.
[28] M.A Bradford, Strength of compact steel beams with partial restraint, Journal of Constructional Steel Research 2000; **53**(2): 183-200.
[29] E. Ellobody, Interaction of buckling modes in castellated steel beams, Journal of Constructional Steel Research 2011; **67**(5): 814-825.
[30] E. Ellobody, Nonlinear analysis of cellular steel beams under combined buckling modes, Thin-Walled Structures 2012; **52**: 66-79.
[31] B. Kim, L.Y. Li, A. Edmonds, Analytical solutions of lateral-torsional buckling of castellated beams, International Journal of Structural Stability and Dynamics 2016;**16**(8): 1-16 (1550044).

[32] J. Zhu, L.Y. Li, A stiffened plate buckling model for calculating critical stress of distortional buckling of CFS beams, International Journal of Mechanical Sciences 2016; **115-116**: 457-464.
[33] X.H. Huang, J. Zhu, A stiffened-plate buckling model for calculating critical stress of distortional buckling of CFS columns, International Journal of Mechanical Sciences 2016; **119**: 237-242.
[34] W.B. Yuan, N.T. Yu, L.Y. Li, Distortional buckling of perforated cold-formed steel channel-section beams with circular holes in web, International Journal of Mechanical Sciences 2017; **126**: 255-260.

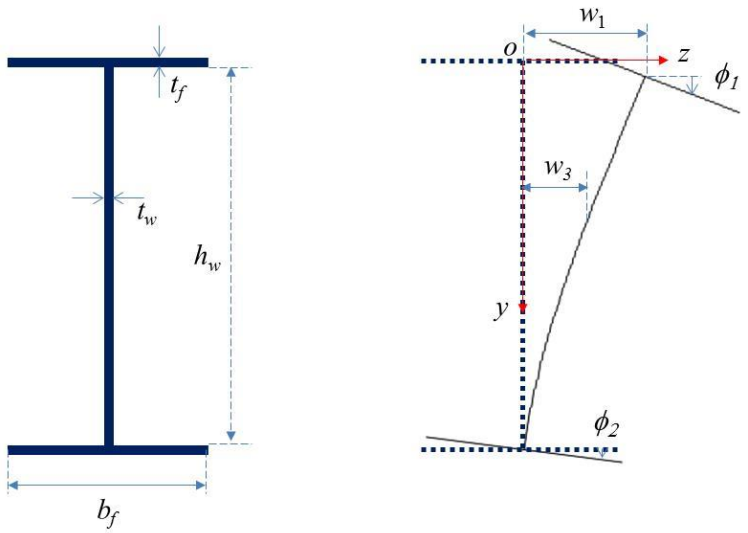

(a) (b)

Figure 1. (a) Symbols used to define sectional dimensions of I-beam. (b) Model used for describing web distortional buckling.

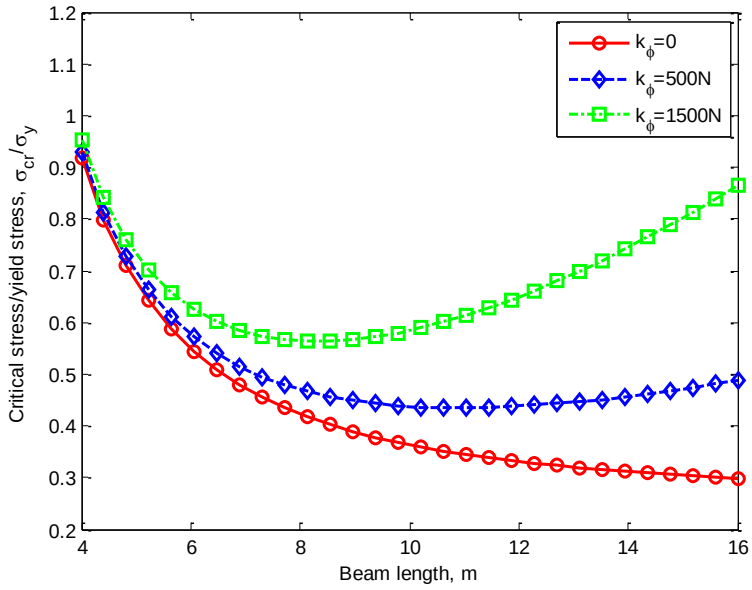

Figure 2. Critical stress of web-flange distortional buckling of a I-section beam (h_w = 350 mm, b_f = 150 mm, t_w = 10 mm, t_f = 10 mm, σ_y = 300 MPa, $\alpha = \beta = 0$).

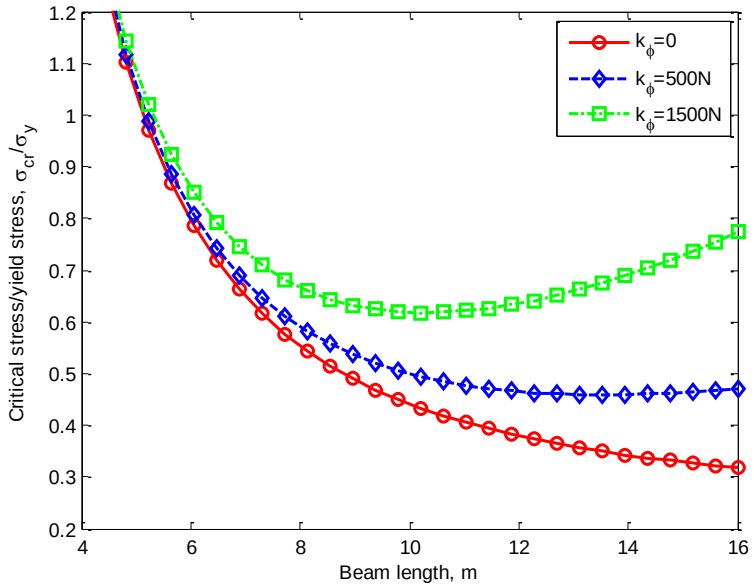

Figure 3. Critical stress of web-flange distortional buckling of a I-section beam (h_w = 350 mm, b_f = 200 mm, t_w = 10 mm, t_f = 10 mm, σ_y = 300 MPa, α = β = 0).

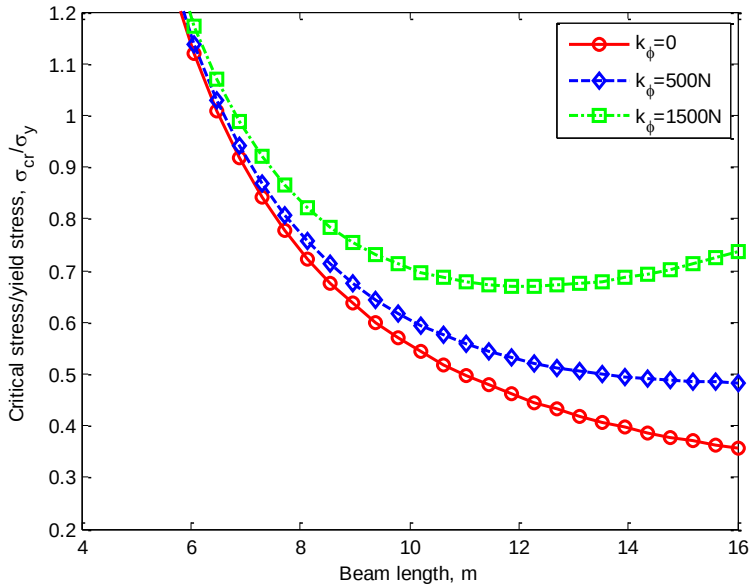

Figure 4. Critical stress of web-flange distortional buckling of a I-section beam (h_w = 350 mm, b_f = 250 mm, t_w = 10 mm, t_f = 10 mm, σ_y = 300 MPa, α = β = 0).

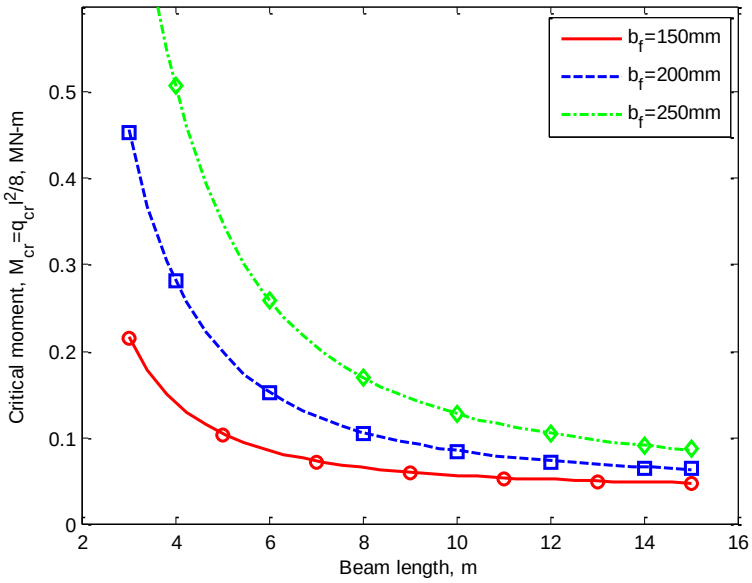

Figure 5. Comparison of critical stresses between present analytical model (dotted-dash, dashed and solid lines) and finite element analysis (diamond, square and circle points) (h_w = 350 mm, t_w = 10 mm, t_f = 10 mm, k_ϕ = 0, σ_y = 300 MPa, α = 1, β = 0).